ELSEVIER

Solid State Ionics 131 (2000) 301–309

SOLID STATE IONICS

www.elsevier.com/locate/ssi

Impedance spectroscopy of (yttria-stabilized zirconia)-magnesia ceramic composites

F.C. Fonseca, R. Muccillo*

Instituto de Pesquisas Energéticas e Nucleares, Comissão Nacional de Energia Nuclear, C.P. 11049, Pinheiros, 05422-970 - S. Paulo, SP, Brazil

Received 20 September 1999; received in revised form 10 April 2000; accepted 17 April 2000

Abstract

$(ZrO_2$:8 mol% $Y_2O_3)_{1-x}$–$(MgO)_x$ ceramic composites have been prepared in the $0 \leq x \leq 0.70$ range by evaporation of a suspension of ZrO_2:8 mol% Y_2O_3 in a solution of magnesium nitrate and ethanol followed by pressing and sintering. The samples were analyzed by X-ray diffraction and scanning electron microscopy. The electrical properties were studied by impedance spectroscopy and analyzed taking into account the contributions due to the different microstructural constituents of the specimens. The results show that the dependence of these contributions to the electrical resistivity on the magnesia content follows two stages: one below and another above the solubility limit of magnesia in yttria-stabilized zirconia. The same dependence is found for the lattice parameter determined by X-ray measurements. The impedance diagrams of the composites have been resolved allowing the identification of contributions due to the presence of each microstructural constituent in both stages.

Keywords: Impedance spectroscopy; Ceramic composites; Zirconia–yttria

1. Introduction

Many recent studies of zirconia solid electrolytes, motivated by several applications (SOFCs, oxygen sensors, pumps, etc.), deal with composite materials and co-doped systems [1–6]. Most of these studies try to clarify the following interesting features about electrical conduction mechanisms in zirconia-based solid electrolytes that still remain controversial: the blocking of charge carriers at grain boundaries and microstructural defects (or second phases) [7]; the degradation of electrical conduction in specimens with doping levels higher than stabilizer content for maximum electrical conductivity [8]; the conduction phenomena at space-charge layers [9]; and the silicon oxide scavenging effect by alumina addition [2]. All these phenomena are not yet completely understood. Consequently, the search for improved electrical conductivity, microstructural and thermal stability of zirconia based solid solutions remains a challenge [9]. Systematic studies concerning the influence of impurities, the change in microstructure, and the role played by a dispersed second insulating phase, on bulk and grain boundary transport prop-

*Corresponding author. Tel.: +55-11-816-9343; fax: +55-11-816-9370.

E-mail addresses: cfonseca@net.ipen.br (F.C. Fonseca), muccillo@usp.br (R. Muccillo)

0167-2738/00/$ – see front matter
PII: S0167-2738(00)00683-4

erties are under way to design zirconia-based solid electrolytes with improved electrical performance.

The ZrO_2–Y_2O_3–MgO ternary system has already been studied specially regarding phase diagram, diffusion-induced grain boundary migration, improved thermal stability for oxygen sensors and structural applications of partially stabilized systems [10–14]. Investigations on the electrical properties of this ternary system are seldom found and no work has been reported on the electrical properties of this system in the cubic region of the ternary phase diagram of the zirconium oxide solid solution.

Impedance spectroscopy can be used to separate the contributions to the electrical resistivity in solid materials; these contributions are due mainly to grains (bulk) and to the different internal surfaces like grain boundaries, pores and second phases [15]. The electrical response of polycrystalline yttria-stabilized zirconia (YSZ) in the electrolytic region, determined by impedance spectroscopy in the Hz to MHz frequency region shows two semicircles [15]: the one at high frequencies is the characteristic response of the bulk, also denoted intragranular response; the other at low frequencies is related to processes that occur in the internal surfaces of polycrystalline specimens with partial blocking of charge carriers, also denoted intergranular response. Blocking processes lead to modifications in the impedance response caused by the presence of blocking regions. A blocking region is a non-conducting or a low-conductivity zone, as far as charge carrier transport is concerned, such as grain boundaries, intergranular or intragranular insulating inclusions and other microstructural defects like pores or cracks [16]. These microstructural features, hereafter named blockers, may cause similar distortions in the YSZ impedance diagram, with an associated characteristic semicircle [17]. The related electrical parameters determined from this semicircle, namely the electrical resistivity, the dielectric constant and the thermal activation energy for ionic conduction, are not ascribed to blocker (MgO in this case) properties, but instead to distortions in the ion conducting matrix properties. In this study magnesia blocking is considered the effect of the presence of magnesia (beyond the solubility limit) on the zirconia–yttria matrix ionic conduction. Blockers are considered able to immobilize a fraction of charge carriers because of the substantial constrictions and blocking of electrical current lines. In this case, an increase in the total electrical resistance is expected [18].

Impedance diagrams of YSZ samples with controlled additions of insulating second phases (such as alumina [19]) or microstructural defects (such as pores [20]) show a larger increase in the low frequency semicircle than in the high frequency one. That means that the main effect of adding insulating second phases to zirconia solid electrolytes is to increase the electrical resistance of the internal surfaces of the electrolyte. The increase in the low frequency electrical resistance characterizes the blocking of charge carriers and depends on the amount of blockers. The blocking factor (α_R) is defined as the ratio of the electrical resistance due to blockers (R_{blockers}) and the total electrical resistance (R_{total}). This parameter is proportional to the fraction of blocked charge carriers and does not depend on sample geometry [16].

Impedance diagrams of materials containing two types of blockers (such as pores and grain boundaries or insulating second phase and grain boundaries) may simultaneously exhibit a third semicircle in a frequency region between the bulk and the grain boundary regions [18,21].

The purpose of this work is to study the electrical properties of solid electrolyte (*cubic zirconia:yttria*)–insulator (*magnesia*) ceramic composites using the impedance spectroscopy technique.

2. Experimental

The starting materials were ZrO_2:8 mol% Y_2O_3 (yttria fully stabilized zirconia from Nissan, Japan) and hydrated magnesium nitrate (Vetec Química Fina, Brazil). The metallic impurities content of the YSZ powder was determined by spectrographic analysis. Silicon and aluminum, known to modify the electrical resistivity of zirconia [22,23], were found in concentrations lower than the detection limit of the technique (60 ppm); the magnesium content was less than 45 ppm.

Samples of $(ZrO_2$:8 mol% $Y_2O_3)_{1-x}$–$(MgO)_x$, with the nominal MgO relative concentration varying from 0 to 70 mol%, were prepared by evaporation of

a suspension of ZrO_2:8 mol% Y_2O_3 in a solution of $Mg(NO_3)_2 \cdot 6\ H_2O$ and ethanol. The evaporation was slowly carried out during mixing at 60°C. This mixture was heated at 500°C for 1 h and the resulting powder was ground in an agate mortar.

Cylindrical pellets were prepared by uniaxial and isostatic pressing at 100 MPa and 200 MPa, respectively, followed by sintering at 1350°C for 0.1 h in air. That temperature was chosen because it is the temperature of maximum densification according to dilatometric results. The short sintering time was used to avoid grain growth. The specimens were analyzed by X-ray diffraction (Bruker AXS D8 Advance and Philips X'pert diffractometers), using Cu K_α radiation. Polished and thermally etched surfaces were observed in a LEO 440i scanning electron microscope for microstructural characterization. Average grain sizes were determined by the Saltykov method using the Quantikov software [24].

The electrical properties were determined by impedance spectroscopy in the 5 Hz to 13 MHz frequency range between 300 and 600°C with an HP 4192A LF impedance analyzer connected to an HP 362 controller. An inconel-600 sample chamber with type S thermocouple and platinum leads was used inside a resistive furnace. Silver paste electrodes were applied to the specimens and cured at 400°C.

3. Results and discussion

Fig. 1 shows X-ray diffraction patterns of $(ZrO_2$:8 mol% $Y_2O_3)_{1-x}$–$(MgO)_x$ composites. All specimens show diffraction peaks corresponding to cubic zirconia. For nominal MgO concentrations higher than 10 mol% the diffraction peaks due to cubic magnesium oxide are detected.

The lattice parameters of cubic zirconia was determined for all compositions [25]. Fig. 2 shows the dependence of the lattice parameter on the magnesia nominal content. A straight line showing the dependence of the calculated lattice parameter of (yttria + magnesia) cubic zirconia solid solution is also included [26]. The values of the lattice parameter as a function of the MgO content decrease linearly down to approximately 10 mol% MgO (in good agreement with calculated values) to a constant value for larger amounts of the insulating phase. This

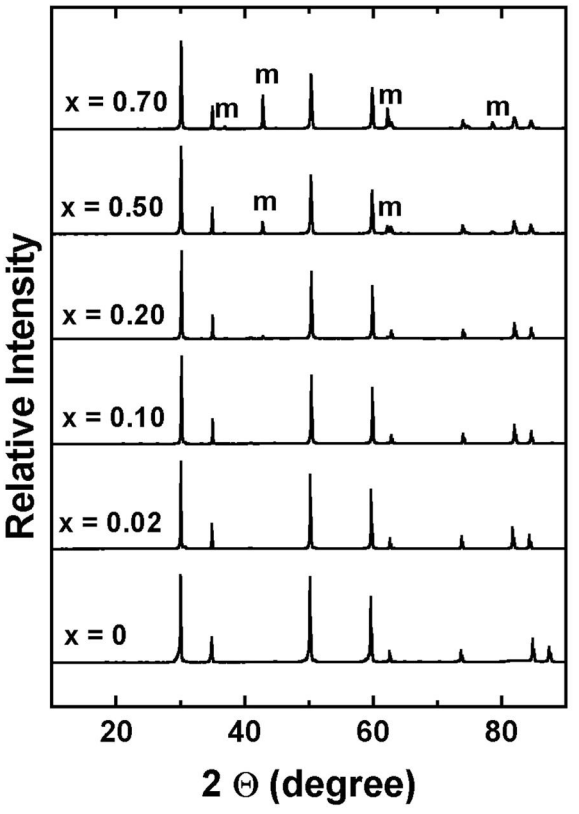

Fig. 1. X-ray diffraction patterns of $(ZrO_2$:8 mol% $Y_2O_3)_{1-x}$–$(MgO)_x$ for $x=0$, 0.02, 0.10, 0.20, 0.50 and 0.70; the main diffraction lines of the cubic magnesia are marked as '**m**'.

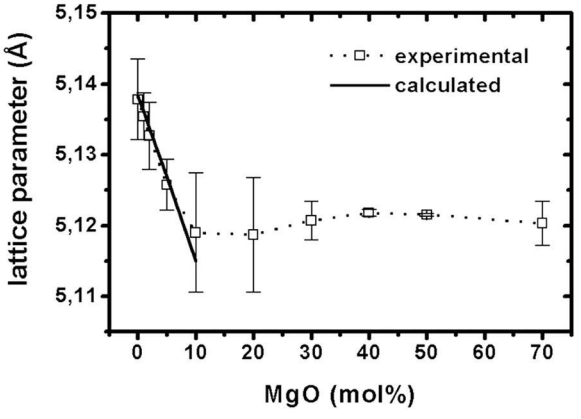

Fig. 2. Values of lattice parameter of cubic zirconia as a function of magnesia molar content and calculated lattice parameter for the yttria + magnesia cubic solid solution [22].

might be an indication that the solubility limit of magnesia in the yttria-fully stabilized zirconia is approximately 10 mol% MgO. Similar results have been reported for ZrO_2:8 mol% Y_2O_3 with Al_2O_3 additions (cf. Fig. 1 in Ref. [6]).

It is already known that for concentrations up to approximately 10 mol%, magnesia as well as yttria stabilizes the cubic structure of zirconium oxide; for magnesia concentrations higher than 10 mol%, the magnesia in excess is found in the specimens as a second phase, characterizing then the composite specimens: (magnesia + yttria)-fully stabilized zirconia and magnesium oxide. This observation is in agreement with the ternary phase diagrams for ZrO_2–Y_2O_3–MgO [10].

Fig. 3 shows scanning electron microscope micrographs of (ZrO_2:8 mol% Y_2O_3)$_{1-x}$–$(MgO)_x$ for $x = 0$, 0.02, 0.10 and 0.30. It can be observed that the specimens are dense with low intergranular porosity, and that increasing the magnesia concentration increases the porosity. The average grain size increases with increasing magnesia addition up to approximately 10 mol% and decreases for concentrations higher than the magnesia solubility limit. The average grain sizes for (ZrO_2:8 mol% Y_2O_3)$_{1-x}$–$(MgO)_x$ for $x = 0$, 0.02, 0.10 and 0.30 are 0.46($\pm$0.19) μm, 0.69($\pm$0.30) μm, 1.60($\pm$0.78) μm and 0.57($\pm$0.22) μm, respectively. Magnesia as a second phase (i.e. having concentrations higher than approximately 10 mol%) in YSZ acts as grain

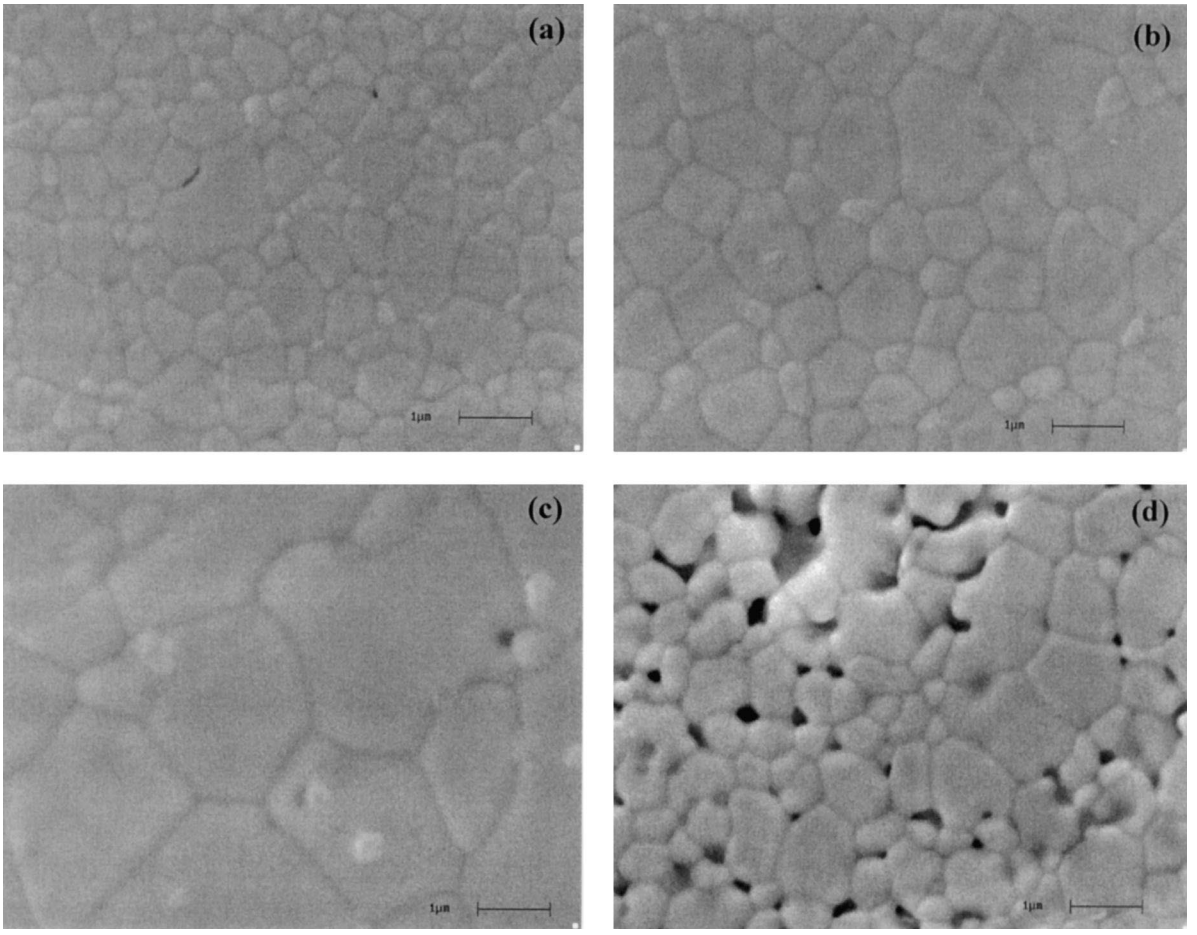

Fig. 3. Electron scanning microscopy micrographs of (ZrO_2:8 mol% Y_2O_3)$_{1-x}$–$(MgO)_x$ samples for $x = 0$ (a), 0.02 (b), 0.10 (c) and 0.30 (d).

growth inhibitor in a manner similar to alumina [23]. The dependence of the grain boundary conductivity on the grain size has already been studied [27–30]. The main conclusion is that the grain boundary conductivity increases with increasing grain size. The analysis of these results leads us to conclude that the large variations in the electrical resistivity reported here should not be due to the observed differences in average grain sizes (see Figs. 4 and 5).

Fig. 4 shows impedance diagrams of $(ZrO_2$:8 mol% $Y_2O_3)_{1-x}$–$(MgO)_x$ measured at 450°C. These diagrams are a further proof that the addition of magnesia can be analyzed according to two stages. The impedance diagrams of samples with concentration up to 5 mol% MgO (Fig. 4a–c) show two well defined semicircles; one at the high frequencies' region, related to bulk or intragranular properties, and another at the low frequencies, related to grain boundary properties [15]. For magnesia concentrations above the solubility limit of 10 mol% MgO (Fig. 4d–g), there is a variation in the shape of the impedance diagrams: a large increase in the high frequency semicircle occurs whilst the low frequency semicircles are progressively overlapped for increasing MgO addition. The impedance diagram of the 70 mol% MgO specimen (Fig. 4g) apparently shows only one semicircle (meaning a complete overlapping of the semicircles found in specimens with less than 70% MgO content); a detailed analysis of the data points at the high frequency end of the impedance diagram of Fig. 4g shows a deviation from a semicircle. As a consequence of that deviation, this diagram could be properly resolved using a two semicircle model, one in the high frequency region and a large one in an intermediate frequency region.

A careful deconvolution analysis of the impedance data of the ceramic composites has been done: three semicircles were obtained for the impedance diagrams of specimens with magnesia concentrations of 10 mol% and higher – the high frequency semicircle (HF) being related to cubic stabilized zirconia grains, the intermediate frequency (IF) to magnesia blocking and the low frequency (LF) to grain boundaries. Even though there are intergranular pores in some specimens (see for example Fig. 3d), pore contribution was not taken into account. For magnesia concentrations lower than 10 mol% the IF semicircle could not be resolved, because magnesia is dissolved in the zirconia–yttria matrix. The LF semicircle of the 70 mol% MgO composition could not be resolved because of the overlapping of both LF and IF contributions.

One of the reasons for following the three semicircle model for resolving the impedance diagrams is that the dependence of parameters like electrical resistivity (Fig. 5), apex frequency (Fig. 6) and dielectric constant (Fig. 7) upon MgO content follows the expected behavior. Another point to be emphasized is the good agreement for fitted parameters of the IF semicircle for all specimens. This is an indication that the blocking regions responsible for the IF semicircle are intergranular MgO. The behavior of the blocking parameters determined using the three semicircle model agrees with the reported behavior of these parameters in YSZ [20]. Even though a 10 mol% magnesia concentration could not be detected by X-ray diffraction (cf. Fig. 1), it could be evaluated by impedance spectroscopy, assuming that after the solid solubility limit, magnesia is present as an intergranular second phase.

Fig. 5 shows values of electrical resistivity of $(ZrO_2$:8 mol% $Y_2O_3)_{1-x}$–$(MgO)_x$ as a function of magnesia content measured at 450°C. The magnesia additions change the electrical resistivity in such a way that two stages, below and above 10 mol% magnesia, could be considered. A large increase of bulk and grain boundary electrical resistivities is observed for increasing the MgO content in the former. This effect can be explained by the fact that the amount of stabilizer being added to cubic zirconia is larger than the stabilizer content for maximum electrical conductivity. Cubic zirconia is known to exhibit a maximum value of electrical conductivity for stabilizer concentrations near the zirconia-rich boundary of the cubic phase [8]. Here, the amount of yttria in the cubic zirconia (8 mol%) provides a solid electrolyte with a maximum value of electrical conductivity. Consequently, the increase in the stabilizer content (now magnesia) causes a decrease in the electrical conductivity. This decrease is usually ascribed to defect interactions [8]. The decrease of the grain boundary conductivity might also be due to the presence of low concentrations of magnesia at the grain boundaries.

The dependence of the total electrical resistivity upon the magnesia content, for magnesia concen-

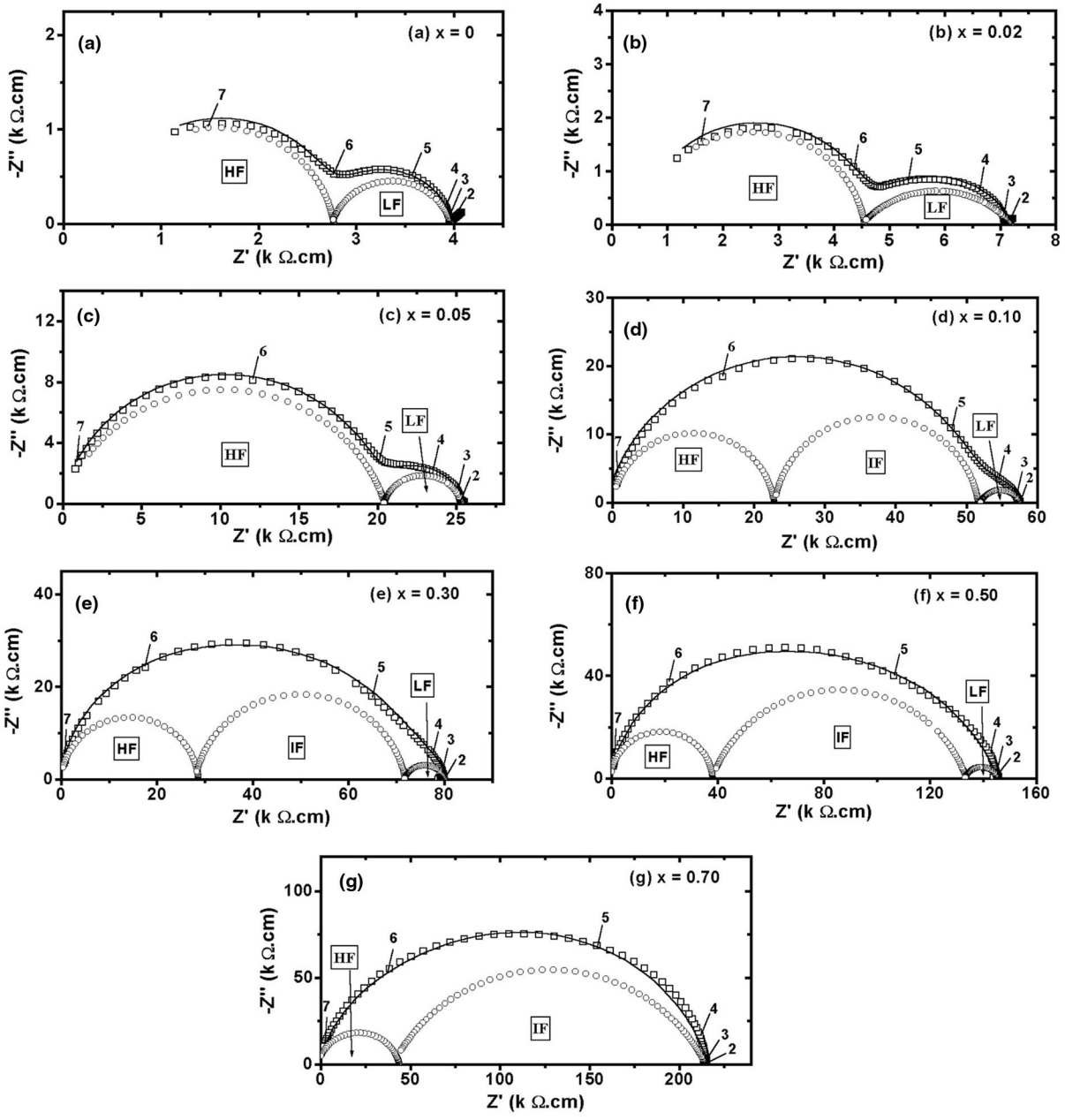

Fig. 4. Impedance diagrams of $(ZrO_2{:}8\ mol\%\ Y_2O_3)_{1-x}$–$(MgO)_x$ samples, for $x=0$ (a), 0.02 (b), 0.05 (c), 0.10 (d), 0.30 (e), 0.50 (f) and 0.70 (g) at 450°C. □ represents the experimental diagrams, — the fitted diagrams and ○ the resolved semicircle arcs.

trations larger than 10 mol%, is the same of a conductor-insulator composite; in this case, magnesia blocking (its response in the impedance diagrams corresponds to the IF semicircle) is the major responsible for the increase in the total electrical resistivity; moreover, the increase in the bulk and grain boundary resistivities of stabilized zirconia (HF semicircle and LF semicircle, respectively) are less

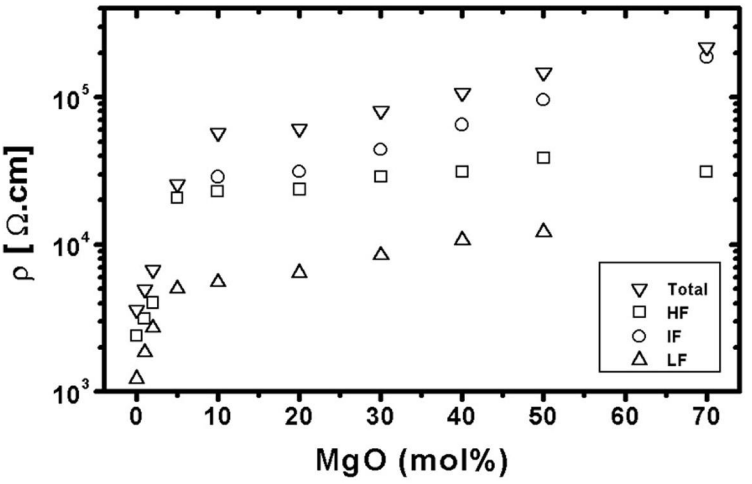

Fig. 5. Electrical resistivity of $(ZrO_2{:}8\ mol\%\ Y_2O_3)_{1-x}$–$(MgO)_x$ as a function of MgO molar content at 450°C.

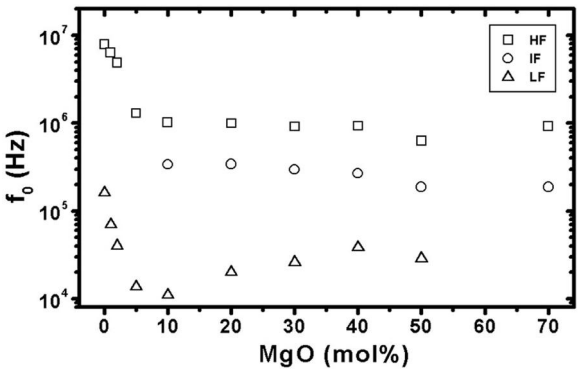

Fig. 6. Relaxation frequency of $(ZrO_2{:}8\ mol\%\ Y_2O_3)_{1-x}$–$(MgO)_x$ as a function of MgO molar content at 450°C.

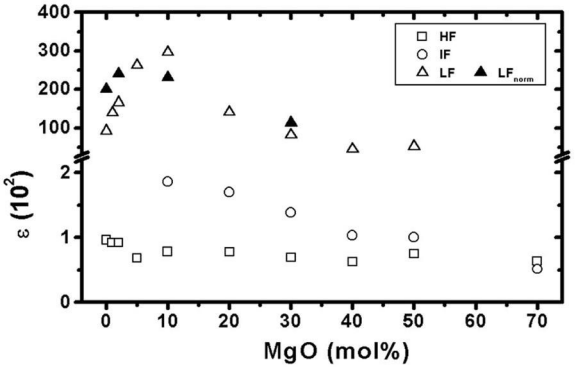

Fig. 7. Dielectric constant of $(ZrO_2{:}8\ mol\%\ Y_2O_3)_{1-x}$–$(MgO)_x$ as a function of MgO molar content at 450°C. The grain boundary dielectric constant values are normalized for the average grain size value for compositions $x = 0$, 0.02, 0.10 and 0.30 mol% MgO (▲).

noticeable. The observed increase in the resistivity, determined by the diameter of the HF semicircle, is similar to the already reported increase of the bulk resistivity of stabilized zirconia with controlled additions of blockers like alumina and pores; it is probably related to the decrease of the volume fraction of cubic grains [16]. No large variations in the total electrical resistivity values as a function of the insulator phase content are observed, indicating that the composite has not yet reached the magnesia percolation threshold.

Activation energies for electrical conduction were calculated using Arrhenius plots. The activation energy values, taking into account all compositions, for the high frequency region (related to bulk conduction in cubic zirconia), intermediate frequency region (to intergranular magnesia blocking in the zirconia matrix) and the low frequency region (to grain boundary in cubic zirconia) are $E_{HF} = 1.15(\pm 0.09)$ eV, $E_{IF} = 1.38(\pm 0.10)$ eV and $E_{LF} = 1.28(\pm 0.16)$ eV, respectively. The value determined for the bulk conduction is in good agreement with the known data for bulk conduction in stabilized zirconia [31]. The values of activation energy determined for the blocking due to magnesia and grain boundary (intermediate IF and low frequency LF semicircles) are higher, within the accepted range for

oxygen ion conduction, and strengthens the supposition that the blockers have similar electrical behavior [16]. The small deviation in the determined values of the activation energies are also an indication that the adopted procedure (three semicircle model) for deconvolution of the impedance diagrams is indeed correct.

Another important parameter in an impedance diagram is the relaxation frequency, the frequency (f_0) in the apex of a semicircle. This parameter can be used as a 'fingerprint' of the relaxing species [21]. Fig. 6 shows the dependence of the relaxation frequency on the magnesia content for the three resolved semicircles of the impedance diagrams measured at 450°C. The HF and LF relaxation frequency values show a behavior similar to the behavior of the lattice parameter (cf. Fig. 2): a decrease for less than 10 mol% magnesia and a constant value for larger concentrations (above the solubility limit). The values of the relaxation frequency derived from the IF semicircle do not depend on the magnesia composition. These results are further proof that the (magnesia + yttria) stabilized zirconia with magnesia additions can have their contributions to the impedance diagrams well resolved even though their characteristic relaxation frequencies differ by less than two orders of magnitude.

Moreover, dielectric constants were determined using the equations $\omega_0 RC = 1$ and $\epsilon = C\epsilon_0(S/l)$; ω_0 is the angular relaxation frequency, R is the electrical resistivity, C is the specific capacitance, ϵ is the dielectric constant, ϵ_0 is the vacuum dielectric constant (8.8542×10^{-14} F cm^{-1}), S is the electrode surface area and l is the sample thickness. Fig. 7 shows the dependence of the dielectric constant on the magnesia addition to yttria-stabilized zirconia. The dielectric constant of the bulk (HF semicircle) is approximately constant over the entire concentration range with an average value of 78($\pm$12), in good agreement with the accepted values for zirconia [32]. The dielectric constant values associated to magnesia blocking (IF semicircle) are higher than that of zirconia [33]. The dielectric constant associated to grain boundaries shows a maximum around 10 mol% magnesia. This behavior can be explained by the grain size variation, since both grain size and grain boundary capacitance show an approximately three-fold increase comparing pure zirconia–yttria with zirconia–yttria with 10 mol% magnesia addition [29]. The values of the grain boundary capacitance were normalized by dividing by the respective average grain size of each composition.

4. Conclusions

The electrical parameters determined in the impedance diagrams of $(ZrO_2$:8 mol% $Y_2O_3)_{1-x}$–$(MgO)_x$ composites can be analyzed taking into account two stages depending on the magnesia content: (a) below approximately 10 mol% magnesia, there is a solubility of magnesium oxide into yttria-stabilized zirconia and (b) above approximately 10 mol% magnesia, the specimen has two distinct phases, namely, (magnesia + yttria) fully stabilized zirconia (ionic conductor) and magnesia (insulator). Impedance spectroscopy can then be used to characterize the electrical properties of both stages. Moreover, it could be proposed as a complementary technique for studying solid solubility limits in doped ceramic oxides.

Acknowledgements

The authors gratefully acknowledge FAPESP (Projects nos. 97/00727-3 and 97/8417-3), CNPq (Proc. 306496/88-7) and PRONEX. Thanks are also due to the Institute of Geological Sciences of the University of S. Paulo for SEM analyses and to Dr. E.N.S. Muccillo for helpful comments.

References

[1] H. Yamamura, N. Utsunomiya, T. Mori, T. Atake, Solid State Ionics 107 (1998) 185.
[2] X. Guo, Solid State Ionics 96 (1997) 247.
[3] M.T. Colomer, P. Durán, A. Caballero, J.R. Jurado, Mater. Sci. Eng. A229 (1997) 114.
[4] L.M. Navarro, P. Recio, P. Duran, J. Mat. Sci. 30 (1995) 1931.
[5] L.M. Navarro, P. Recio, P. Duran, J. Mat. Sci. 30 (1995) 1939.
[6] L.M. Navarro, P. Recio, J.R. Jurado, P. Duran, J. Mat. Sci. 30 (1995) 1949.

[7] L. Dessemond, R. Muccillo, M. Hénault, M. Kleitz, Appl. Phys. A 57 (1993) 57.
[8] J.F. Baumard, P. Abelard, in: N. Claussen, M. Rühle, A.H. Heuer (Eds.), Science and Technology of Zirconia II, Advances in Ceramics, Vol. 12, The American Ceramic Society, Columbus, Ohio, USA, 1983, pp. 555–571.
[9] M. Filal, C. Petot, M. Mokchah, C. Chateau, J.L. Carpentier, Solid State Ionics 80 (1995) 27.
[10] J.R. Hellmann, V.S. Stubican, J. Am. Ceram. Soc. 66 (1983) 265.
[11] R.K. Slotwinski, N. Bonanos, E.P. Butler, J. Mater. Sci. Lett. 4 (1985) 641.
[12] J.-W. Jeong, D.-Y. Yoon, J.-Y. Lee, D.-Y. Kim, J. Am. Ceram. Soc. 75 (1992) 2659.
[13] O.T. Sørensen, M.E.S. Ali, Solid State Ionics 49 (1991) 155.
[14] Z. Jin, Y. Du, Ceram. Int. 20 (1994) 17.
[15] J. Bauerle, J. Phys. Chem. Solids 30 (1969) 2657.
[16] M. Kleitz, L. Dessemond, M.C. Steil, Solid State Ionics 75 (1995) 107.
[17] M. Kleitz, M.C. Steil, J. Eur. Ceram. Soc. 17 (1997) 819.
[18] M. Kleitz, L. Dessemond, M.C. Steil, F. Thevenot, in: R.A. Gerhardt, S.R. Taylor, E.J. Garboczi (Eds.), Mat. Res. Symp. Proc., Vol. 411, 1996, p. 269.
[19] M.C. Steil, F. Thévenot, L. Dessemond, M. Kleitz, in: Third Euro – Ceramics, Madrid, Spain, Vol. 2, 1993, p. 271.
[20] M.C. Steil, F. Thévenot, M. Kleitz, J. Electrochem. Soc. 144 (1997) 390.
[21] E.N.S. Muccillo, M. Kleitz, J. European Ceram. Soc. 16 (1996) 453.
[22] E.P. Butler, R.K. Slotwinski, N. Bonanos, J. Drennan, B.C.H. Steele, in: N. Claussen, M. Rühle, A.H. Heuer (Eds.), Science and Technology of Zirconia II, Advances in Ceramics, Vol. 12, The American Ceramic Society, Columbus, Ohio, USA, 1983, pp. 572–584.
[23] S. Rajendran, J. Drennan, S.P.S. Badwal, J. Mater. Sci. Lett. 6 (1987) 1431.
[24] L.S. Martins Pinto, Ph.D. Thesis, IPEN-USP, S. Paulo, Brazil, 1996.
[25] R.P. Ingel, D. Lewis III, J. Am. Ceram. Soc. 69 (1986) 325.
[26] J.-W. Jeong, D.N. Yoon, J. Am. Ceram. Soc. 73 (1990) 2063.
[27] A.I. Ioffe, M.V. Inozemtzev, A.S. Lipilin, M.V. Perfilev, S.V. Karpachov, Phys. Stat. Sol. (a) 30 (1975) 87.
[28] H. Bernard, Ph.D. Thesis, Institut National Polytéchnique de Grenoble, Grenoble, 1980.
[29] S.H. Chu, M.A. Seitz, J. Sol. St. Chem. 23 (1978) 287.
[30] M.J. Verkerk, B.J. Middelhuis, A.J. Burggraaf, Solid State Ionics 6 (1982) 159.
[31] F.T. Ciacchi, K.M. Crane, S.P.S. Badwal, Solid State Ionics 73 (1994) 49.
[32] E.N.S. Muccillo, M. Kleitz, J. European Ceram. Soc. 15 (1995) 51.
[33] A.R. Von Hippel, Dielectric Materials and Applications, 2nd Edition, Artech House, Boston, 1954.